Modeling and Propulsion Methods of Underwater Snake Robots

E. Kelasidi, K. Y. Pettersen, J. T. Gravdahl, S. Strømsøyen, and A.J. Sørensen

Abstract— In this paper we consider underwater snake robots (USRs) that may be equipped with additional added effectors along their body, including caudal, dorsal and pectoral fins, tunnel thrusters and/or a stern propeller. We propose a mathematical model for USRs swimming in a 2D plane, which includes the extra propulsion forces acting on each link from the added effectors. The resulting model is in closed form, making it well-suited for control design and analysis. We then consider the particular case when fins are added to one or more links to provide lift forces. We develop a quasi-static model for an oscillating and rotating foil, which is then combined with the model of the USR to provide a model of an USR with one or more fins along its body. This makes it possible to make a simulation-based comparison of the USR energy efficiency with and without fins. Simulation results presented in this paper show that there is a significant improvement in propulsion efficiency for the USR with a caudal (tail) fin compared to the results obtained for the USR without a caudal fin.

I. INTRODUCTION

Unmanned underwater vehicles (UUVs) are increasingly used for mapping and monitoring of the seabead and for different challenging applications where inspection and intervention tasks are required in subsea structures. In particular, different types of UUVs such as conventional work class remotely operated vehicles (ROVs), inspection class ROVs and autonomous underwater vehicles (AUVs) are now widely used for subsea inspection, maintenance, and repair (IMR) operations in the oil and gas industry, archaeology, oceanography and marine biology [1], [2], [3]. In addition, lately, research has been conducted on developing intervention AUVs (I-AUVs) [4], underwater snake robots (USRs) [5], [6] and underwater swimming manipulators (USMs) [2], [3] as alternative solutions for several tasks to be performed in the subsea environment, with an overall goal to overcome and extend the capabilities of existing UUVs in the future.

USRs and USMs are particularly interesting since their flexible and slender shape may offer a range similar to a torpedo-shaped AUV, and maneuverability and access capabilities exceeding those of inspection class ROVs. In addition, the USR/USM is a manipulator arm capable of doing light intervention tasks, thus providing intervention capabilities that AUVs and inspection class ROVs cannot

provide. Furthermore, the bio-motivated USR and USM offer the potential of increased propulsion efficiency in transit and maneuvering, which is an important aspect for the energy autonomy of UUVs. In particular, sea snakes, eels and fish have through evolution developed very efficient propulsion and locomotion methods. In particular, they have high efficiency and maneuverability performance, as they are able to change direction rapidly with negligible loss in kinetic energy and some of them have outstanding acceleration capabilities [7], [8], [9]. For instance a tuna fish is able to achieve an acceleration that exceeds the gravity 20 times [10], [11]. Eels and sea snakes are able to swim both forward and backward, while their flexible body makes it possible to swim in confined spaces. In addition, bio-inspired solutions can be less noisy than using propeller, which can be an important factor for several applications subsea. Consequently, in this paper, we investigate if it is

Fig. 1: Underwater snake robots capable of both inspection and light intervention tasks.

possible to combine the properties of aquatic animals with the best solutions from marine technology in one robot, capable of both inspection and light intervention tasks (See Fig. 1). In particular, it is interesting to investigate whether it is possible to build a new type of biologically inspired swimming robot, which combines the incredible locomotion efficiency of biological fish and the well-known marine propeller propulsion solutions, with the potential to increase flexibility, maneuverability and locomotion efficiency. The underwater snake robot studied in this paper is a slender multi-articulated robot, which is able to propel itself forward by using body undulations combined with caudal, dorsal and pectoral fins and/or with stern propeller and tunnel thrusters along the body.

The mathematical model of the USR is more challenging compared to models of ROVs and AUVs, because of its multi-articulated body. There are several models proposed for swimming snake-like robots. A discussion of the different modeling approaches proposed for USRs can be found in [5], [12]. This paper proposes a closed form model for USRs

swimming in a 2D plane, which takes into account the extra propulsion forces acting along the body when the snake robot is equipped with different added effectors, such as a caudal tail, fins, stern propeller, and tunnel thrusters, in addition to the propulsion forces generated by the link angle motion together with the hydrodynamic forces. The model of a USM moving in a 2D plane presented in [1] modifies the kinematic equations and the equations of motion developed for a USR in [12] to accommodate the different mass and length of each link, and to take into account the forces from additional effectors. In this paper, the hydrodynamic model presented in [1] and [12] is extended to model the added mass effects more accurately, which then is combined with the kinematic model to derive a closed form model of the USR. In addition, analytical expressions for the fluid parameters, which take into account the different values of the fluid coefficients and geometry of each link, are derived.

Furthermore, being inspired by biological creatures, in this paper we investigate foil propulsion combined with the propulsion from body undulations of the USR, with an overall goal of improving efficiency, speed and maneuvering characteristics of the bioinspired swimming snake robots. A quasi-static model for an oscillating and rotating foil is proposed and combined with the equation of motion of the USR. This gives the opportunity to add a fin to one or more links of the snake robot and obtain comparison simulation results with and without fins. Simulation studies in this paper with and without a caudal fin show a significant reduction in the work per meter for the USR with caudal fin at the same forward velocities. To the authors' best knowledge, this is the first closed form model of an underwater snake robot with added fins, which makes it possible to combine the maneuverability of the biological eel with the tail fin that provides the outstanding acceleration and efficiency of tuna fish, and the additional thrusters from marine technology that can provide both extra speed and hovering capabilities. The paper is organized as follows. The kinematics, hydrodynamics and the dynamics of a USR is presented in Section II. In Section III, the quasi-static foil model is presented and combined with the model of the USR. Simulation results with and without a caudal fin are presented in Section IV, followed by concluding remarks in Section V.

II. MODEL OF USR WITH ADDED EFFECTORS

This section presents the kinematic and dynamic model for USRs with added effectors, including an extended model of the hydrodynamic forces. In addition, analytical expressions for the fluid parameters considering different values of the fluid coefficients and geometry of the each link are derived.

A. Notations and Defined Symbols

In this paper we consider a USR with n rigid links. Each link has the length $2l_i$, where i indicates the link number. The links are assumed to have mass m_i and moment of inertia $J_i = \frac{1}{3}m_i l_i^2$. The mass of each link is uniformly distributed so that the link center of mass (CM) is located in the midpoint. The total mass of the robot is defined as the sum of the mass of all the links, $m_t = \sum_{i=1}^n m_i$. The

TABLE I: Definition of mathematical terms

Symbol	Description	Vector
n	The number of links	
l_i	The half length of a link	$\mathbf{L} \in \mathbb{R}^{n \times n}$
m_i	Mass of each link	$\mathbf{M} \in \mathbb{R}^{n \times n}$
J_i	Moment of inertia of each link	$\mathbf{J} \in \mathbb{R}^{n \times n}$
θ_i	Angle between link i and the global x axis	$\theta \in \mathbb{R}^n$
ϕ_i	Angle of joint i	$\phi \in \mathbb{R}^{n-1}$
(x_i, y_i)	Global coordinates of the CM of link i	$\mathbf{X}, \mathbf{Y} \in \mathbb{R}^n$
(p_x, p_y)	Global coordinates of the CM of the robot	$\mathbf{p}_{CM} \in \mathbb{R}^2$
u_i	Actuator torque of joint between link i and link $i+1$	$\mathbf{u} \in \mathbb{R}^{n-1}$
u_{i-1}	Actuator torque of joint between link i and link $i-1$	$\mathbf{u} \in \mathbb{R}^{n-1}$
$(f_{x,i}, f_{y,i})$	Fluid force on link i	$\mathbf{f_x}, \mathbf{f_y} \in \mathbb{R}^n$
τ_i	Fluid torque on link i	$\tau \in \mathbb{R}^n$
$(f_{tx,i}, f_{ty,i})$	Propulsive force on link i	$\mathbf{f_{tx}}, \mathbf{f_{ty}} \in \mathbb{R}^n$
$\tau_{t,i}$	Torque from propulsive force on link i	$\tau_t \in \mathbb{R}^n$
$(h_{x,i}, h_{y,i})$	Joint constraint force on link i from link $i+1$	$\mathbf{h_x}, \mathbf{h_y} \in \mathbb{R}^{n-1}$
$-(h_{x,i-1}, h_{y,i-1})$	Joint constraint force on link i from link $i-1$	$\mathbf{h_x}, \mathbf{h_y} \in \mathbb{R}^{n-1}$

links of the USR (numbered from $i = 1$ to $i = n$ from tail to head) are interconnected by $n-1$ motorized joints. The parameter $\theta_i \in \mathbb{R}$ denotes the *link angle* of each link $i \in 1, \ldots, n$ of the robot, while the *joint angle* of joint $i \in 1, \ldots, n-1$ is given by $\phi_i = \theta_i - \theta_{i+1}$. The link and the joint angles are grouped in vectors $\theta = [\theta_1, \ldots, \theta_n]^T \in \mathbb{R}^n$ and $\phi = [\phi_1, \ldots, \phi_{n-1}]^T \in \mathbb{R}^{n-1}$, respectively. Table I gives the description of the symbols used to derive the model in the following sections. For the derivation of the proposed model, the following vectors and matrices are used:

$$\mathbf{A} = \begin{bmatrix} 1 & 1 & & \\ & \ddots & \ddots & \\ & & 1 & 1 \end{bmatrix}, \mathbf{D} = \begin{bmatrix} 1 & -1 & & \\ & \ddots & \ddots & \\ & & 1 & -1 \end{bmatrix},$$

where $\mathbf{A}, \mathbf{D} \in \mathbb{R}^{(n-1) \times n}$. Furthermore, $\bar{\mathbf{D}} = \mathbf{D}^T (\mathbf{D}\mathbf{D}^T)^{-1}$,

$$\mathbf{e} = \begin{bmatrix} 1, & \cdots, & 1 \end{bmatrix}^T \in \mathbb{R}^n, \mathbf{E} = \begin{bmatrix} \mathbf{e} & \mathbf{0}_{n \times 1} \\ \mathbf{0}_{n \times 1} & \mathbf{e} \end{bmatrix} \in \mathbb{R}^{2n \times 2},$$

$$\sin\theta = \begin{bmatrix} \sin\theta_1, \ldots, \sin\theta_n \end{bmatrix}^T \in \mathbb{R}^n,$$

$$\cos\theta = \begin{bmatrix} \cos\theta_1, \ldots, \cos\theta_n \end{bmatrix}^T \in \mathbb{R}^n$$

$$\mathbf{S}_\theta = \text{diag}(\sin\theta) \in \mathbb{R}^{n \times n}, \qquad \mathbf{C}_\theta = \text{diag}(\cos\theta) \in \mathbb{R}^{n \times n}$$

$$\dot{\theta}^2 = \begin{bmatrix} \dot{\theta_1}^2, & \cdots, & \dot{\theta_n}^2 \end{bmatrix}^T \in \mathbb{R}^n,$$

$$\mathbf{M} = \text{diag}(m_1, \ldots, m_n) \in \mathbb{R}^{n \times n}, \mathbf{L} = \text{diag}(l_1, \ldots, l_n) \in \mathbb{R}^{n \times n},$$

$$\mathbf{J} = \text{diag}(J_1, \ldots, J_n) \in \mathbb{R}^{n \times n}, \bar{\mathbf{K}} = \mathbf{L}\mathbf{A}^T (\mathbf{D}\mathbf{M}^{-1}\mathbf{D}^T)^{-1}\mathbf{D}\mathbf{M}^{-1},$$

$$\bar{\mathbf{V}} = \mathbf{L}\mathbf{A}^T (\mathbf{D}\mathbf{D}^T)^{-1}\mathbf{D}, \quad \mathbf{V}_1 = \bar{\mathbf{V}}\mathbf{M}\bar{\mathbf{K}}^T, \quad \mathbf{V}_2 = \bar{\mathbf{V}}\mathbf{M}\mathbf{e}.$$

B. Kinematics of Underwater Snake Robot

This section briefly presents the model of the kinematics of a USR moving in a virtual horizontal plane previously presented in [1], [9] for completeness of the paper. The snake robot is considered to have $n+2$ degrees of freedom (n link angles and the x-y position of the robot). The position $\mathbf{p}_{CM}$ of the CM is given by

$$\mathbf{p}_{CM} = \begin{bmatrix} p_x \\ p_y \end{bmatrix} = \begin{bmatrix} \frac{1}{m_t} \sum_{i=1}^n m_i x_i \\ \frac{1}{m_t} \sum_{i=1}^n m_i y_i \end{bmatrix} = \frac{1}{m_t} \begin{bmatrix} \mathbf{e}^T \mathbf{M}\mathbf{X} \\ \mathbf{e}^T \mathbf{M}\mathbf{Y} \end{bmatrix}, \quad (1)$$

where $\mathbf{X} = [x_1, \ldots, x_n]^T \in \mathbb{R}^n$ and $\mathbf{Y} = [y_1, \ldots, y_n]^T \in \mathbb{R}^n$ are given by

$$\mathbf{X} = -\bar{\mathbf{K}}^T \cos\theta + \mathbf{e}p_x \quad \mathbf{Y} = -\bar{\mathbf{K}}^T \sin\theta + \mathbf{e}p_y. \quad (2)$$

In addition, the linear velocities and the accelerations of the links are given by

$$\dot{\mathbf{X}} = \bar{\mathbf{K}}^T \mathbf{S}_\theta \dot{\theta} + \mathbf{e}\dot{p}_x \quad \dot{\mathbf{Y}} = -\bar{\mathbf{K}}^T \mathbf{C}_\theta \dot{\theta} + \mathbf{e}\dot{p}_y, \quad (3)$$

and

$$\ddot{\mathbf{X}} = \bar{\mathbf{K}}^T \left(\mathbf{C}_\theta \dot{\theta}^2 + \mathbf{S}_\theta \ddot{\theta} \right) + \mathbf{e}\ddot{p}_x$$

$$\ddot{\mathbf{Y}} = \bar{\mathbf{K}}^T \left(\mathbf{S}_\theta \dot{\theta}^2 - \mathbf{C}_\theta \ddot{\theta} \right) + \mathbf{e}\ddot{p}_y, \quad (4)$$

respectively. More details regarding the derivation of the kinematics can be found in [1], [9].

C. Hydrodynamic Modeling

In [1], [12], for a neutrally buoyant USR considering that the fluid is viscid, incompressible, and irrotational in the inertia frame and that the current is constant and irrotational in the inertial frame, it is shown that the fluid forces on all links can be expressed in vector form as

$$\mathbf{f} = \begin{bmatrix} \mathbf{f_x} \\ \mathbf{f_y} \end{bmatrix} = \begin{bmatrix} \mathbf{f_{D_x}^I} \\ \mathbf{f_{D_y}^I} \end{bmatrix} + \begin{bmatrix} \mathbf{f_{D_x}^{II}} \\ \mathbf{f_{D_y}^{II}} \end{bmatrix}, \tag{5}$$

where $\mathbf{f_{D_x}^I}$, $\mathbf{f_{D_y}^I}$ and $\mathbf{f_{D_x}^{II}}$, $\mathbf{f_{D_y}^{II}}$ represent the effects from the linear and nonlinear drag forces, respectively, and are given by

$$\begin{bmatrix} \mathbf{f_{D_x}^I} \\ \mathbf{f_{D_y}^I} \end{bmatrix} = -\begin{bmatrix} \mathbf{c}_T \mathbf{C}_\theta & -\mathbf{c}_N \mathbf{S}_\theta \\ \mathbf{c}_T \mathbf{S}_\theta & \mathbf{c}_N \mathbf{C}_\theta \end{bmatrix} \begin{bmatrix} \mathbf{V}_{\mathbf{r_x}} \\ \mathbf{V}_{\mathbf{r_y}} \end{bmatrix}, \tag{6}$$

$$\begin{bmatrix} \mathbf{f_{D_x}^{II}} \\ \mathbf{f_{D_y}^{II}} \end{bmatrix} = -\begin{bmatrix} \mathbf{c}_T \mathbf{C}_\theta & -\mathbf{c}_N \mathbf{S}_\theta \\ \mathbf{c}_T \mathbf{S}_\theta & \mathbf{c}_N \mathbf{C}_\theta \end{bmatrix} \mathrm{sgn}\left(\begin{bmatrix} \mathbf{V}_{\mathbf{r_x}} \\ \mathbf{V}_{\mathbf{r_y}} \end{bmatrix} \right) \begin{bmatrix} \mathbf{V}_{\mathbf{r_x}}^2 \\ \mathbf{V}_{\mathbf{r_y}}^2 \end{bmatrix}, \tag{7}$$

with the relative velocities in the body frame given by

$$\begin{bmatrix} \mathbf{V}_{\mathbf{r_x}} \\ \mathbf{V}_{\mathbf{r_y}} \end{bmatrix} = \begin{bmatrix} \mathbf{C}_\theta & \mathbf{S}_\theta \\ -\mathbf{S}_\theta & \mathbf{C}_\theta \end{bmatrix} \begin{bmatrix} \dot{\mathbf{X}} - \mathbf{V}_x \\ \dot{\mathbf{Y}} - \mathbf{V}_y \end{bmatrix}, \tag{8}$$

where $\mathrm{sgn}(\mathbf{x}) = \mathrm{diag}(x_1, \cdots, x_{2n}) \in \mathbb{R}^{2n \times 2n}$, for $\mathbf{x} \in \mathbb{R}^{2n}$, $\mathbf{V}_{(\cdot)}^2 = \begin{bmatrix} V_{(\cdot)_1}^2, \ldots, V_{(\cdot)_n}^2 \end{bmatrix}^T \in \mathbb{R}^n$, $\mathbf{V}_x = \mathbf{e}V_x \in \mathbb{R}^n$ and $\mathbf{V}_y = \mathbf{e}V_y \in \mathbb{R}^n$ where V_x and V_y are the ocean current velocities in the inertial x and y direction, respectively, and where $\mathbf{c}_T = \mathrm{diag}(c_{T,1}, \ldots, c_{T,n}) \in \mathbb{R}^{n \times n}$ and $\mathbf{c}_N = \mathrm{diag}(c_{N,1}, \ldots, c_{N,n}) \in \mathbb{R}^{n \times n}$ represent the drag parameters due to the pressure difference between the two sides of the body in the tangent and normal direction of each link.

The relative accelerations of the links in body frame can be found by differentiating (8) with respect to time, which gives

$$\begin{bmatrix} \dot{\mathbf{V}}_{\mathbf{r_x}} \\ \dot{\mathbf{V}}_{\mathbf{r_y}} \end{bmatrix} = \begin{bmatrix} \mathbf{C}_\theta & \mathbf{S}_\theta \\ -\mathbf{S}_\theta & \mathbf{C}_\theta \end{bmatrix} \begin{bmatrix} \ddot{\mathbf{X}} \\ \ddot{\mathbf{Y}} \end{bmatrix}$$
$$+ \begin{bmatrix} -\mathbf{S}_\theta & \mathbf{C}_\theta \\ -\mathbf{C}_\theta & -\mathbf{S}_\theta \end{bmatrix} \begin{bmatrix} \mathrm{diag}(\dot{\theta}) & \mathbf{0} \\ \mathbf{0} & \mathrm{diag}(\dot{\theta}) \end{bmatrix} \begin{bmatrix} \dot{\mathbf{X}} - \mathbf{V}_x \\ \dot{\mathbf{Y}} - \mathbf{V}_y \end{bmatrix}. \tag{9}$$

Following step by step the procedure presented in [12] and using the equation of the relative acceleration in body frame (9) derived in this paper, the vectors $\mathbf{f_{A_x}}$ and $\mathbf{f_{A_y}}$ representing the added mass effects can be expressed as

$$\begin{bmatrix} \mathbf{f_{A_x}} \\ \mathbf{f_{A_y}} \end{bmatrix} = -\begin{bmatrix} \mathbf{C}_\theta & -\mathbf{S}_\theta \\ \mathbf{S}_\theta & \mathbf{C}_\theta \end{bmatrix} \begin{bmatrix} \mathbf{0} & \mathbf{0} \\ \mathbf{0} & \mu \end{bmatrix} \begin{bmatrix} \dot{\mathbf{V}}_{\mathbf{r_x}} \\ \dot{\mathbf{V}}_{\mathbf{r_y}} \end{bmatrix}, \tag{10}$$

where $\mu = \mathrm{diag}(\mu_1, \ldots, \mu_n) \in \mathbb{R}^{n \times n}$. The parameters μ_i represent the added mass for each link of the fluid carried by the moving body. Here, we assume that the USR is operating deeply submerged below the wave zone. Hence, constant values for added mass are assumed (asymptotic values when wave frequency is going to zero). Furthermore, as shown in [1], the fluid torques on all links are given by

$$\tau = -\Lambda_1 \ddot{\theta} - \Lambda_2 \dot{\theta} - \Lambda_3 \dot{\theta}|\dot{\theta}|, \tag{11}$$

where $\Lambda_1 = \mathrm{diag}(\lambda_{1,1}, \ldots, \lambda_{1,n}) \in \mathbb{R}^{n \times n}$, $\Lambda_2 = \mathrm{diag}(\lambda_{2,1}, \ldots, \lambda_{2,n}) \in \mathbb{R}^{n \times n}$ and $\Lambda_3 = \mathrm{diag}(\lambda_{3,1}, \ldots, \lambda_{3,n}) \in \mathbb{R}^{n \times n}$. The coefficients $\lambda_{2,i}$, $\lambda_{3,i}$ represent the drag torque parameters, and the parameter $\lambda_{1,i}$ represents the added mass parameter.

Based on the same concept used in [12] for robots consisting of identical links, the hydrodynamic related parameters for the cylindrical links with major diameter $2e_{1i}$ and minor diameter $2e_{2i}$, and taking into account that the length of each link is $2l_i$, can be expressed as follows

$$c_{T,i} = \frac{1}{2}\rho\pi C_f \frac{(e_{2i}+e_{1i})}{2}2l_i, \quad c_{N,i} = \frac{1}{2}\rho C_D 2e_{1i}2l_i,$$
$$\mu_i = \rho\pi C_A e_{1i}^2 2l_i, \quad \lambda_{1,i} = \frac{1}{12}\rho\pi C_M (e_{1i}^2 - e_{2i}^2)^2 l_i^3, \tag{12}$$
$$\lambda_{2,i} = \frac{1}{6}\rho\pi C_f (e_{1i}+e_{2i})l_i^3, \quad \lambda_{3,i} = \frac{1}{8}\rho\pi C_f (e_{1i}+e_{2i})l_i^4,$$

for $i \in 1, \ldots, n$ where C_f and C_D are the drag coefficients in the body-fixed x and y direction of the links, while C_A denotes the added mass coefficient, C_M is the added inertia coefficient and ρ is the density of the fluid [12].

Remark 1: Note that by mistake some terms were omitted in the added mass model in [1] and [12], [13]. These terms are included in the hydrodynamic model given by (5). In particular, analytical equations of the added mass forces are derived using a more general expression for the relative accelerations, (9).

D. Forces from Added Effectors

In [1], it is shown that the forces from added effectors along the snake robot can be expressed in the global frame as

$$\mathbf{f_{tx}} = \mathbf{B_x}^T \mathbf{f_t} \in \mathbb{R}^n, \qquad \mathbf{B_x}(\mathbf{b_x}) \in \mathbb{R}^{r \times n}$$
$$\mathbf{f_{ty}} = \mathbf{B_y}^T \mathbf{f_t} \in \mathbb{R}^n, \qquad \mathbf{B_y}(\mathbf{b_y}) \in \mathbb{R}^{r \times n}, \tag{13}$$

where the configuration vectors $\mathbf{b_x} = [\cos(\theta_{k_1} + \xi_{k_1}), \cos(\theta_{k_2} + \xi_{k_2}), \ldots, \cos(\theta_{k_r} + \xi_{k_r})]^T$ and $\mathbf{b_y} = [\sin(\theta_{k_1} + \xi_{k_1}), \sin(\theta_{k_2} + \xi_{k_2}), \ldots, \sin(\theta_{k_r} + \xi_{k_r})]^T$ are defined as the x and y components of the added effector forces of link i represented in the global frame, and

$$\mathbf{f}_{t,i} = \begin{bmatrix} \cos(\theta_i + \xi_i) \\ \sin(\theta_i + \xi_i) \end{bmatrix} f_{t,i}, \tag{14}$$

where ξ_i represents the direction of the added force vector with respect to the local reference frame, and $f_{t,i}$ represents the scalar magnitude of the effector forces of link i. Furthermore, r is the total number of additional effectors and $k_i \in (1, n)$.

Remark 2: Note that the model in (13) is general since it can be used to include any kind of added effector forces, e.g. fins, caudal tail, tunnel thrusters and/or a stern propeller, depending on the application.

E. Equations of Motion

This section presents the resulting equations of motion for the underwater snake robot. In [1],[9], it is shown that the force balance equation for all links of a USR with different link mass and length can be expressed as

$$\mathbf{M\ddot{X}} = \mathbf{D}^T \mathbf{h_x} + \mathbf{f_x} + \mathbf{f_{tx}}, \quad \mathbf{M\ddot{Y}} = \mathbf{D}^T \mathbf{h_y} + \mathbf{f_y} + \mathbf{f_{ty}}, \tag{15}$$

where $\mathbf{f_x}$ and $\mathbf{f_y}$ are the fluid forces derived in Section II.C in the x and y direction, respectively, and $\mathbf{f_{tx}}, \mathbf{f_{ty}}$ are the forces from the added effectors derived in Section II.D. Furthermore, the acceleration of the CM of the robot is given by [1],[9]

$$\begin{bmatrix} \ddot{p}_x \\ \ddot{p}_y \end{bmatrix} = \frac{1}{m_t} \begin{bmatrix} \mathbf{e}^T & \mathbf{0} \\ \mathbf{0} & \mathbf{e}^T \end{bmatrix} \begin{bmatrix} \mathbf{f_x} + \mathbf{f_{tx}} \\ \mathbf{f_y} + \mathbf{f_{ty}} \end{bmatrix}, \tag{16}$$

where m_t is the total mass of the robot. By inserting (5), (10), (9), (3) and finally (4) into (16), we are able to obtain the following equation for the acceleration of the CM of the robot:

$$\begin{bmatrix} \ddot{p}_x \\ \ddot{p}_y \end{bmatrix} = -\mathbf{M_p}\mathbf{N_p} \begin{bmatrix} \text{diag}(\dot{\theta}) & \mathbf{0} \\ \mathbf{0} & \text{diag}(\dot{\theta}) \end{bmatrix} \mathbf{E} \begin{bmatrix} \dot{p}_x \\ \dot{p}_y \end{bmatrix}$$
$$- \mathbf{M_p}\mathbf{N_p} \begin{bmatrix} \text{diag}(\dot{\theta}) & \mathbf{0} \\ \mathbf{0} & \text{diag}(\dot{\theta}) \end{bmatrix} \begin{bmatrix} \bar{\mathbf{K}}^T\mathbf{S}_\theta\dot{\theta} - \mathbf{V_x} \\ -\bar{\mathbf{K}}^T\mathbf{C}_\theta\dot{\theta} - \mathbf{V_y} \end{bmatrix} \quad (17)$$
$$- \mathbf{M_p}\mathbf{L_p} \begin{bmatrix} \bar{\mathbf{K}}^T(\mathbf{C}_\theta\dot{\theta}^2 + \mathbf{S}_\theta\ddot{\theta}) \\ \bar{\mathbf{K}}^T(\mathbf{S}_\theta\dot{\theta}^2 - \mathbf{C}_\theta\ddot{\theta}) \end{bmatrix} + \mathbf{M_p}\mathbf{E}^T \begin{bmatrix} \mathbf{f_{Dx}} + \mathbf{f_{tx}} \\ \mathbf{f_{Dy}} + \mathbf{f_{ty}} \end{bmatrix},$$

where $\mathbf{f_{Dx}} = \mathbf{f_{D_x}^I} + \mathbf{f_{D_x}^{II}}$ and $\mathbf{f_{Dy}} = \mathbf{f_{D_y}^I} + \mathbf{f_{D_y}^{II}}$ representing the drag forces in the x and y direction, and the matrices $\mathbf{M_p}$, $\mathbf{N_p}$ and $\mathbf{L_p}$ are given in Appendix A.

Additionally, the torque balance equation is given by [9]

$$\mathbf{J}\ddot{\theta} = \mathbf{D}^T\mathbf{u} - \mathbf{S}_\theta\mathbf{L}\mathbf{A}^T\mathbf{h_x} + \mathbf{C}_\theta\mathbf{L}\mathbf{A}^T\mathbf{h_y} + \tau + \tau_\mathbf{t}, \quad (18)$$

where τ is given by (11) and $\tau_\mathbf{t}$ represents the fluid torques from the added effectors. The joint constraint forces can be obtained by multiplying (15) by $\mathbf{D}$ and solving for $\mathbf{h_x}$ and $\mathbf{h_y}$:

$$\mathbf{h_x} = (\mathbf{D}\mathbf{D}^T)^{-1}\mathbf{D}(\mathbf{M}\ddot{\mathbf{X}} - \mathbf{f_x} - \mathbf{f_{tx}})$$
$$\mathbf{h_y} = (\mathbf{D}\mathbf{D}^T)^{-1}\mathbf{D}(\mathbf{M}\ddot{\mathbf{Y}} - \mathbf{f_y} - \mathbf{f_{ty}}). \quad (19)$$

By inserting (19), (4) and (5) into (18), we get

$$(\mathbf{J} + \mathbf{S}_\theta\mathbf{V_1}\mathbf{S}_\theta + \mathbf{C}_\theta\mathbf{V_1}\mathbf{C}_\theta)\ddot{\theta} - (-\mathbf{S}_\theta\mathbf{V_1}\mathbf{C}_\theta + \mathbf{C}_\theta\mathbf{V_1}\mathbf{S}_\theta)\dot{\theta}^2$$
$$= \mathbf{D}^T\mathbf{u} - \mathbf{S}_\theta\mathbf{V_2}\ddot{p}_x + \mathbf{C}_\theta\mathbf{V_2}\ddot{p}_y + \mathbf{S}_\theta\bar{\mathbf{V}}\mathbf{f_{Ax}} - \mathbf{C}_\theta\bar{\mathbf{V}}\mathbf{f_{Ay}} \quad (20)$$
$$+ \mathbf{S}_\theta\bar{\mathbf{V}}(\mathbf{f_{Dx}} + \mathbf{f_{tx}}) - \mathbf{C}_\theta\bar{\mathbf{V}}(\mathbf{f_{Dy}} + \mathbf{f_{ty}}) + \tau + \tau_\mathbf{t},$$

By inserting (10), (17) and finally (11) into (20), we are able to express the rotational equation of motion of the robot as follows:

$$\mathbf{M}_\theta\ddot{\theta} + \mathbf{W}_\theta\dot{\theta}^2 + \mathbf{V}_{\theta,\dot{\theta}}\dot{\theta} + \mathbf{N}_{\theta,\dot{\theta}}(\mathbf{e}\dot{p}_x - \mathbf{V_x}) + \mathbf{P}_{\theta,\dot{\theta}}(\mathbf{e}\dot{p}_y - \mathbf{V_y})$$
$$+ \mathbf{K_x}(\mathbf{f_{Dx}} + \mathbf{f_{tx}}) + \mathbf{K_y}(\mathbf{f_{Dy}} + \mathbf{f_{ty}}) - \tau_\mathbf{t} = \mathbf{D}^T\mathbf{u}, \quad (21)$$

where $\mathbf{u} \in \mathbb{R}^{n-1}$ is the control input, and the matrices $\mathbf{M}_\theta$, $\mathbf{W}_\theta$, $\mathbf{V}_{\theta,\dot{\theta}}$, $\mathbf{N}_{\theta,\dot{\theta}}$ $\mathbf{P}_{\theta,\dot{\theta}}$, $\mathbf{K_x}$ and $\mathbf{K_y}$ are given in Appendix A.

Remark 3: Note that the model (17), (21) is general and can also be used to model propulsive forces for land-based snake robots with motorized legs or wheels, if we disregard the added mass effects and use the ground friction model in [14] instead of the drag forces. The concept of having different configurations of a land-based snake robot with motorized propulsive legs or wheels is presented in [15].

Remark 4: For the special case where the links of the robot have the same mass and length, $\bar{\mathbf{K}}$ and $\bar{\mathbf{V}}$ reduce to $\bar{\mathbf{K}} = \bar{\mathbf{V}} = l\mathbf{K}$ where $\mathbf{K} = \mathbf{A}^T(\mathbf{D}\mathbf{D}^T)^{-1}\mathbf{D}$. Furthermore, $\mathbf{V_1}$ and $\mathbf{V_2}$ reduce to $\mathbf{V_1} = ml^2\mathbf{V}$ and $\mathbf{V_2} = ml\mathbf{K}\mathbf{e}$ where $\mathbf{V} = \mathbf{A}^T(\mathbf{D}\mathbf{D}^T)^{-1}\mathbf{A}$.

III. Quasi-Static Foil Model

A foil, which generates lift forces, is one alternative for added effectors along the USR body. In this section we develop a model of a foil, which can then be combined with the model of the USR developed in Section II to study alternative propulsion methods for USRs. Most of the modeling approaches proposed so far for USRs omit to include a model of extra propulsive modules such as fins

or thrusters, and it will be interesting to study a robot that combines the manuverability capabilities and the flexibility of anguilliform swimmers (such as eels/snakes), and the high efficiency and speed characteristics of tunniform swimmers mostly due to their caudal fin (such as tunas) into one underwater robot.

Studies of aquatic swimming animals have shown that there are three dominant mechanisms that are responsible for the propulsion of these animals: drag forces, added mass forces and forces due to lift effects. In addition, it is shown that drag forces are dominant for the anguilliform mode, lift forces generated by foils are dominant for the tunniform mode, while in between the added mass forces are dominating [16], [17]. For the modeling of swimming fish-like robots, Lighthill's elongated-body theory is commonly used [7], which considers only the added mass effects as important for the propulsion of the robot [16], [18]. However, later studies have showed that also the lift forces contribute to the propulsion of different types of swimmers [16], [17]. Therefore, in this paper, we propose a model for a foil where both the added mass and lift forces are included. There are three analytical methods for modeling lift on a foil: steady lift, quasi-steady and unsteady lift. It is commonly accepted that the lift forces on an aquatic swimmer are not steady, but most likely unsteady [16], [17]. The Theodorsen's and Wagner's methods are commonly used for calculating the lift forces on an unsteady flat plate [19]. These methods are, however, quite complex and not easy to solve analytically. Therefore, in this paper, a quasi-static foil model is used to model the lift and the added mass forces on a foil. Note that a quasi-static model can be combined with the closed-form model of a USR from Section II, avoiding the numerical calculations of lift, and thus keeping the property of being a closed form analytical model. This is an important property, making the model suitable for analysis and control design.

Motivated by the approach presented in [19] for airfoil dynamics, we can show that the forces and torques from n foils can be expressed as

$$\mathbf{L_f} = \pi\rho\mathbf{S}\left(\mathbf{B}^2\ddot{\mathbf{h}} + \mathbf{B}^2U\dot{\delta} - \mathbf{B}^3\alpha\ddot{\delta}\right)$$
$$+ \mathbf{S}2\pi\rho U^2\mathbf{B}\left(\delta + \text{atan}(\frac{\dot{\mathbf{h}}}{U}) + \text{atan}\left(\mathbf{B}\left(\frac{1}{2}\mathbf{I}_n - \alpha\right)\frac{\dot{\delta}}{U}\right)\right)$$
$$\mathbf{M_f} = -\mathbf{S}\pi\rho\left(\mathbf{B}^3\left(\frac{1}{2}\mathbf{I}_n - \alpha\right)U\dot{\delta} + \mathbf{B}^4\left(\frac{1}{8}\mathbf{I}_n + \alpha^2\right)\ddot{\delta} - \mathbf{B}^3\alpha\ddot{\mathbf{h}}\right)$$
$$+ \mathbf{S}2\pi\rho U^2\left(\alpha + \frac{1}{2}\mathbf{I}_n\right)\mathbf{B}^2\left(\delta + \text{atan}\left(\frac{\dot{\mathbf{h}}}{U}\right) + \text{atan}\left(\mathbf{B}\left(\frac{1}{2}\mathbf{I}_n - \alpha\right)\frac{\dot{\delta}}{U}\right)\right), \quad (22)$$

where the first term is the added mass force and torque, and the second term represents the lifting force and torque. The $n \times n$ matrix $\mathbf{S} = \text{diag}(S_1, \dots, S_n)$ is defined as a diagonal matrix with the total span (i.e. the tip to tip length of the foil) S_i of foil i. This makes it possible to calculate the lift for n foils at the same time. In addition, the vectors $\mathbf{h}$ and δ represent the translation motion and the rotation motion, respectively. The forward velocity of the robot, or in flow velocity to the foil in case of a stationary robot, is denoted as U, the cord c_i is the width of the foil i, and α_i is the

distance between the rotation axis and the mid cord given in semi cords ($b_i = c_i/2$). The half cord matrix is defined by the mean cord of each foil i, as $\mathbf{B} = \mathrm{diag}(b_{\mathrm{mean},1}, \ldots, b_{\mathrm{mean},n})$, where the mean half cord can be calculated as

$$b_{\mathrm{mean,i}} = \frac{1}{r}\sum_{1}^{r} b_j, \tag{23}$$

where r is the number of equal spans that the foil is divided into and $\alpha = \mathrm{diag}(\alpha_1, \ldots, \alpha_n)$. For more details please see [9].

Furthermore, the total drag force is a sum of the induced drag from the tip vortices, D_{Ii}, and the friction drag, D_{fi}, and is expressed as [20], [21], [22]

$$D_{l_i} = D_{I_i} + D_{f_i} = \frac{1}{2}\rho(C_{df_i} + C_{di})A_{ri}U^2, \tag{24}$$

where $A_{ri} = 4S_i b_{\mathrm{mean,i}}$ and the coefficients C_{df_i} and C_{di} are given by

$$C_{df_i} = 2C_{ft}\left(1 + 2\frac{t_{\max,i}}{c_i}\right), \quad C_{di} = \frac{C_{Li}^2}{\pi \mathrm{Asp}_i}, \tag{25}$$

where $C_{ft} = \dfrac{0.075}{(\log R_n - 2)^2}$, R_n is the Reynolds number, the parameter is $t_{\max,i} = 2N_{\mathrm{prof}}b_{\mathrm{mean},i}$, N_{prof} represents the foil profile, $\mathrm{Asp}_i = S_i/2b_{\mathrm{mean},i}$, and the lift coefficients can be calculated according to [9], [20], [21]

$$\mathbf{C_L} = \frac{\pi \mathbf{B}^2 \dot{\delta}}{1/2U}. \tag{26}$$

The drag forces from different foils can be assembled in a vector $\mathbf{D_l} = [D_{l_1}, \ldots, D_{l_N}]$. What remains is to define the terms necessary to merge the foil model with the model of the USR proposed in Section II. First, we choose to define the speed U in (22) as the relative forward speed of the robot in global frame according to

$$U = \sqrt{(\dot{p}_x - v_x)^2 + (\dot{p}_y - v_y)^2}, \tag{27}$$

where v_x and v_y are the ocean current values in the x and y direction of the global frame. Second, the heading (orientation) ψ of the robot is defined as the average of the link angles, i.e. as [23]

$$\psi = \frac{1}{n}\sum_{i=1}^{n}\theta_i. \tag{28}$$

Furthermore, the parameters δ, $\mathbf{h}$ and their derivatives need to be defined as parameters of the robot. Fig. 2 illustrates a foil attache to a link i. Three coordinate systems are define in this figure: F_I representing the global frame coordinate system, F_B corresponding to the body frame coordinate system defined at the CM of link i, and F_a representing the coordinate system with respect to forward velocity $\vec{U}$. Note that δ_i corresponds to the yaw angle of the foil relative to the velocity $\vec{U}$ (see Fig. 2). In this paper, the heading is considered constant, which will simplify the equations of motion significantly. Under this assumption, we are able to define the following expressions for the parameter δ from Fig. 2

$$\delta = \theta - \psi, \quad \dot{\delta} = \dot{\theta}, \quad \ddot{\delta} = \ddot{\theta}. \tag{29}$$

The parameter β_i is the angle between the velocity $\vec{U}$ and the inflow velocity $\vec{V}$ to the foil (see Fig. 2), given by

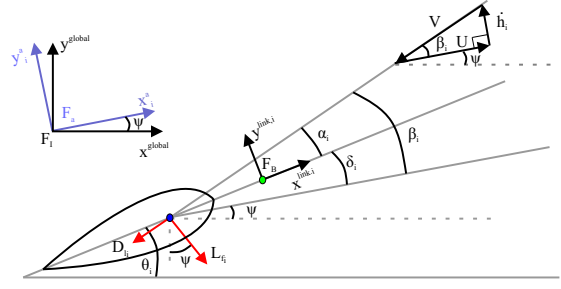$$\beta_i = \mathrm{atan}\left(\frac{\dot{h}_i}{U}\right). \tag{30}$$

Fig. 2: Illustration of the foil, where the green and blue circles represent the CM of link i and the center of pressure that the lift force acts through.

The parameters h_i, $\dot{h}_i$ and $\ddot{h}_i$ can be grouped in vectors $\mathbf{h} = [h_1, \ldots, h_n]^T$, $\dot{\mathbf{h}} = [\dot{h}_1, \ldots, \dot{h}_n]^T$ and $\ddot{\mathbf{h}} = [\ddot{h}_1, \ldots, \ddot{h}_n]^T$, when considering several fins. From Fig. 2, we see that $\mathbf{h}$, $\dot{\mathbf{h}}$ and $\ddot{\mathbf{h}}$ are the y components of the positions, velocities and the accelerations in the F_a coordinate system (i.e. position, velocity and the acceleration of the links of the robot from global frame (F_I) to the coordinate system with respect to U (F_a) given by

$$\begin{aligned}
\mathbf{h} &= \mathbf{S}_\psi \mathbf{X} + \mathbf{C}_\psi \mathbf{Y}, \\
\dot{\mathbf{h}} &= \mathbf{S}_\psi(\dot{\mathbf{X}} - \mathbf{V_x}) + \mathbf{C}_\psi(\dot{\mathbf{Y}} - \mathbf{V_y}), \\
\ddot{\mathbf{h}} &= \mathbf{S}_\psi \ddot{\mathbf{X}} + \mathbf{C}_\psi \ddot{\mathbf{Y}}.
\end{aligned} \tag{31}$$

Finally, by decomposing the lift and drag forces in x and y, we are able to write the forces from the foils as follows:

$$\begin{aligned}
\mathbf{f_{tx}} &= \mathbf{S}_{\beta\psi}\mathbf{L_f} - \mathbf{C}_{\beta\psi}\mathbf{D_l}, \\
\mathbf{f_{ty}} &= \mathbf{C}_{\beta\psi}\mathbf{L_f} + \mathbf{S}_{\beta\psi}\mathbf{D_l}, \\
\tau_\mathbf{f} &= \mathbf{M_f},
\end{aligned} \tag{32}$$

where $\mathbf{C}_{\beta\psi} = \mathrm{diag}\left(\cos(\beta_1 + \psi), \ldots, \cos(\beta_N + \psi)\right)$ and $\mathbf{S}_{\beta\psi} = \mathrm{diag}\left(\sin(\beta_1 + \psi), \ldots, \sin(\beta_N + \psi)\right)$. Using (22) and (32), the equations for the forces and torques can be written as

$$\begin{aligned}
\mathbf{f_{tx}} &= \mathbf{f_{tx}^A} + \mathbf{f_{tx}^R}, \\
\mathbf{f_{ty}} &= \mathbf{f_{ty}^A} + \mathbf{f_{ty}^R}, \\
\tau_\mathbf{t} &= \tau_\mathbf{t}^A + \tau_\mathbf{t}^R,
\end{aligned} \tag{33}$$

where the terms dependent on the acceleration are given by

$$\begin{aligned}
\mathbf{f_{tx}^A} &= \mathbf{S}_{\beta\psi}\pi\rho\mathbf{S}\left(\mathbf{B}^2\ddot{\mathbf{h}} - \mathbf{B}^3\alpha\ddot{\delta}\right), \\
\mathbf{f_{ty}^A} &= \mathbf{C}_{\beta\psi}\pi\rho\mathbf{S}\left(\mathbf{B}^2\ddot{\mathbf{h}} - \mathbf{B}^3\alpha\ddot{\delta}\right), \\
\tau_\mathbf{t}^A &= -\mathbf{S}\pi\rho\left(\mathbf{B}^4\left(\frac{1}{8}\mathbf{I}_n + \alpha^2\right)\ddot{\delta} - \mathbf{B}^3\alpha\ddot{\mathbf{h}}\right),
\end{aligned} \tag{34}$$

while the terms independent on the acceleration are given by

$$\begin{aligned}
\mathbf{f_{tx}^R} &= \mathbf{S}_{\beta\psi}\left(\pi\rho\mathbf{S}(\alpha U\dot{\delta})\right) + \mathbf{S}_{\beta\psi}\mathbf{S}2\pi\rho U^2\mathbf{B}\left(\delta + \mathrm{atan}(\frac{\dot{\mathbf{h}}}{U})\right) \\
&\quad + \mathbf{S}_{\beta\psi}\mathbf{S}2\pi\rho U^2\mathbf{B}\mathrm{atan}\left(\mathbf{B}\left(\frac{1}{2}\mathbf{I}_n - \alpha\right)\frac{\dot{\delta}}{U}\right) - \mathbf{C}_{\beta\psi}\mathbf{D_l}, \\
\mathbf{f_{ty}^R} &= \mathbf{C}_{\beta\psi}\left(\pi\rho\mathbf{S}(\alpha U\dot{\delta})\right) + \mathbf{C}_{\beta\psi}\mathbf{S}2\pi\rho U^2\mathbf{B}\left(\delta + \mathrm{atan}(\frac{\dot{\mathbf{h}}}{U})\right) \\
&\quad + \mathbf{C}_{\beta\psi}\mathbf{S}2\pi\rho U^2\mathbf{B}\mathrm{atan}\left(\mathbf{B}\left(\frac{1}{2}\mathbf{I}_n - \alpha\right)\frac{\dot{\delta}}{U}\right) + \mathbf{S}_{\beta\psi}\mathbf{D_l}, \\
\tau_\mathbf{t}^R &= -\mathbf{S}\pi\rho\mathbf{B}^3\left(\frac{1}{2}\mathbf{I}_n - \alpha\right)U\dot{\delta} + \mathbf{S}2\pi\rho U^2\left(\alpha + \frac{1}{2}\mathbf{I}_n\right) \\
&\quad \mathbf{B}^2\left(\delta + \mathrm{atan}\left(\frac{\dot{\mathbf{h}}}{U}\right) + \mathrm{atan}\left(\mathbf{B}\left(\frac{1}{2}\mathbf{I}_n - \alpha\right)\frac{\dot{\delta}}{U}\right)\right).
\end{aligned} \tag{35}$$

By inserting (34), (33), (31), (29) and finally (4) into (17), we are able to write the acceleration of the CM for the combined model of a USR with the foil model as:

$$
\begin{bmatrix} \ddot{p}_x \\ \ddot{p}_y \end{bmatrix} = -\mathbf{M_p^t N_p} \begin{bmatrix} \mathrm{diag}(\dot{\theta}) & \mathbf{0} \\ \mathbf{0} & \mathrm{diag}(\dot{\theta}) \end{bmatrix} \mathbf{E} \begin{bmatrix} \dot{p}_x \\ \dot{p}_y \end{bmatrix}
$$
$$
- \mathbf{M_p^t N_p} \begin{bmatrix} \mathrm{diag}(\dot{\theta}) & \mathbf{0} \\ \mathbf{0} & \mathrm{diag}(\dot{\theta}) \end{bmatrix} \begin{bmatrix} \bar{\mathbf{K}}^T \mathbf{S}_\theta \dot{\theta} - \mathbf{V_x} \\ -\bar{\mathbf{K}}^T \mathbf{C}_\theta \dot{\theta} - \mathbf{V_y} \end{bmatrix}
$$
$$
- \mathbf{M_p^t}(\mathbf{L_p} + \mathbf{S_p}) \begin{bmatrix} \bar{\mathbf{K}}^T (\mathbf{C}_\theta \dot{\theta}^2 + \mathbf{S}_\theta \ddot{\theta}) \\ \bar{\mathbf{K}}^T (\mathbf{S}_\theta \dot{\theta}^2 - \mathbf{C}_\theta \ddot{\theta}) \end{bmatrix} \quad (36)
$$
$$
- \mathbf{M_p^t K_p} \begin{bmatrix} \ddot{\theta} \\ \ddot{\theta} \end{bmatrix} + \mathbf{M_p^t E}^T \begin{bmatrix} \mathbf{f_{Dx}} + \mathbf{f_{tx}^R} \\ \mathbf{f_{Dy}} + \mathbf{f_{ty}^R} \end{bmatrix},
$$

where $\mathbf{f_{tx}^R}$ and $\mathbf{f_{ty}^R}$ are given by (35). The expressions for the matrices $\mathbf{M_p^t}$, $\mathbf{S_p}$ and $\mathbf{K_p}$ are given in Appendix A.

In addition, the equation of the torque needs to be modified in order to include terms from the foil torque. By inserting (33), (31), (29), (4) and finally (36) into (20), we get

$$
\mathbf{M_\theta^t} \ddot{\theta} + \mathbf{W_\theta^t} \dot{\theta}^2 + \mathbf{V_{\theta,\dot{\theta}}^t} \dot{\theta} + \mathbf{N_{\theta,\dot{\theta}}^t}(\mathbf{e}\dot{p}_x - \mathbf{V_x}) + \mathbf{P_{\theta,\dot{\theta}}^t}(\mathbf{e}\dot{p}_y - \mathbf{V_y})
$$
$$
+ \mathbf{K_x^t}(\mathbf{f_{Dx}} + \mathbf{f_{tx}}) + \mathbf{K_y^t}(\mathbf{f_{Dy}} + \mathbf{f_{ty}}) - \tau_t^R = \mathbf{D}^T \mathbf{u}, \quad (37)
$$

where $\mathbf{f_{tx}^R}$, $\mathbf{f_{ty}^R}$ and τ_t^R are given by (35). The analytical expressions of the matrices $\mathbf{M_\theta^t}$, $\mathbf{W_\theta^t}$, $\mathbf{V_{\theta,\dot{\theta}}^t}$, $\mathbf{N_{\theta,\dot{\theta}}^t}$, $\mathbf{P_{\theta,\dot{\theta}}^t}$, $\mathbf{K_x^t}$ and $\mathbf{K_y^t}$ are given in Appendix A.

IV. SIMULATION STUDY

In this section simulation results are presented to compare the performance of a USR with and without a caudal fin. Both models were simulated using the *ode23tb* solver in *Matlab R2015b* with a relative and absolute error tolerance of 10^{-4}.

A. Joint Control

The following PD-controller was used to calculate the joints' actuator torques from the joints' reference angles:

$$
u_i = \ddot{\phi}_i^* + k_p(\phi_i^* - \phi_i) + k_d(\dot{\phi}_i^* - \dot{\phi}_i), \quad i = 1,\dots,n-1, \quad (38)
$$

where $k_p > 0$ and $k_d > 0$ are the control gains. The reference angle $\phi_i^*(t)$ of each joint $i \in 1,\dots,n-1$ of the underwater snake robot was calculated according to [23]

$$
\phi_i^*(t) = \alpha_h g(i,n) \sin(\omega_h t + (i-1)\delta_h) + \phi_0, \quad (39)
$$

where α_h is the maximum amplitude, ω_h the frequency, and δ_h the phase shift between the joints of the sinusoidal motion pattern. The parameter ϕ_0 is a joint offset [14], [23], and $g(i,n)$ is a scaling function for the joint amplitude along the body. For instance, $g(i,n) = 1$ gives lateral undulation and $g(i,n) = (n-i)/(n+1)$ gives eel-like motion.

B. Simulation Parameters

Simulations were performed for a robot with $n = 10$ links, each one having length $2l_i = 2 \times 0.07$ m. For the simulations of the USR with caudal fin, the first (tail) link was assumed to be a bit longer, having $2l_1 = 2 \times 0.075$, so that it is possible to fit a caudal tail on the link. In order to fulfill the neutrally buoyant property, the mass of each link was assumed to be $m_i = 0.6597$ kg, while the mass of the first link, when considering a robot with caudal fin, was set to $m_1 = 0.7468$ kg. The fluid parameters $c_{T,i}$, $c_{N,i}$, μ_i, $\lambda_{1,i}$, $\lambda_{2,i}$,

and $\lambda_{3,i}$ were computed for $2e_{1i} = 2 \cdot 0.05$ m, $2e_{2i} = 2 \cdot 0.03$ m. The fluid properties were assumed to be $\rho = 1000$ kg/m^3 and $C_f = 0.03$, $C_D = 2$, $C_A = 1$, $C_M = 1$ and used to compute the parameters by using (12). In this paper simulation results were obtained considering a high aspect ratio fin, like the one that tuna and sailfish has, with mean cord $c_1 = 0.0194$ m and span $S_1 = 0.12$, which gives an aspect ratio of 0.62. As we have already mentioned, the caudal fin is attached to the first link of the robot with the lift center ($c_1/4$ from the leading edge) being on the mid point of the link. The distance $\alpha_1 = -0.5 - l_1/b_{\mathrm{mean},1}$ was calculated considering l_1 as the half of the first link length and $b_{\mathrm{mean},1} = c_1/2$. The thickness of the foil was considered to be $N_{\mathrm{prof}} = 0.16$. The gait parameters were set to $\alpha_h = 30^\circ$, $\omega_h = 100^\circ/\text{s}$ and $\delta_h = 40^\circ$, while the control gains were chosen as $k_p = 200$ and $k_d = 50$. For the obtained simulation results the robot was controlled to follow the x axis by using the following P heading controller:

$$
\phi_o = k_\theta (\psi_{\mathrm{ref}} - \psi), \quad (40)
$$

where $k_\theta > 0$ is a control gain [23]. The orientation of the robot was computed according to (28), while the reference orientation was defined using the line-of-sight (LOS) guidance law

$$
\psi_{\mathrm{ref}} = -\arctan\left(\frac{p_y}{\Delta}\right), \quad \Delta > 0 \quad (41)
$$

where p_y is the cross track error and Δ is a constant design parameter that influences the rate of convergence to the desired path. For more details please see [23]. The heading control parameters were set to $k_\theta = 0.1$ and $\Delta = 2\pi l_1$. Note that in the simulations we chose to not consider the ocean current effects. It will be a topic of future work to investigate whether ocean currents have any effect on the energy consumption of motion with fins compared to motion without fins. Hence, the simulation results are presented with $v_x = v_y = 0$.

C. Simulation Results

The time evolution of the position of the CM of the robot with and without the caudal fin is shown in Fig. 3 and Fig. 4 for the lateral undulation and eel-like motion pattern, respectively. From these figures, we can see that the robot with a caudal fin managed to travel a longer distance for both the investigated motion patterns. The average forward velocity was obtained using the following expression:

$$
\bar{v} = \frac{\sqrt{(p_{\mathrm{stop},x} - p_{\mathrm{start},x})^2 + (p_{\mathrm{stop},y} - p_{\mathrm{start},y})^2}}{t_{\mathrm{stop}} - t_{\mathrm{start}}}, \quad (42)
$$

where $\mathbf{p}_{\mathrm{start}}$ and $\mathbf{p}_{\mathrm{stop}}$ represent the initial and the final points of the distance traveled in the time interval $t_{\mathrm{stop}} - t_{\mathrm{start}}$. When using lateral undulation, the robot with a caudal tail achieved the average forward velocity $\bar{v} = 0.2802$m/s, while the robot without the caudal tail achieved the slightly lower velocity $\bar{v} = 0.2312$m/s. For the eel-like motion pattern, the obtained velocity with the caudal tail was $\bar{v} = 0.3573$m/s, while it was significantly lower without the tail: $\bar{v} = 0.1966$m/s. The obtained simulation results have thus showed that the use of a
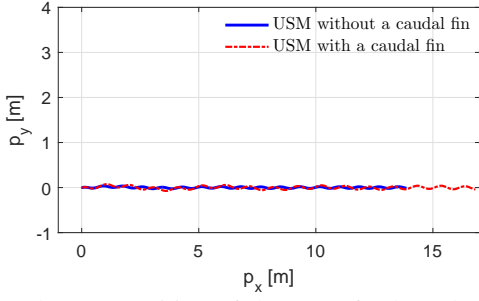
Fig. 3: The CM position of the USR for lateral undulation.
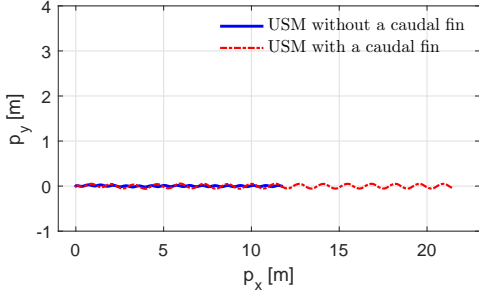

Fig. 4: The CM position of the USR for eel-like motion.

caudal fin increases the velocity for the two investigated motion patterns, lateral undulation and eel-like motion pattern. This is in accordance with the literature on fish propulsion [9]. In addition, simulation results were obtained for the work per meter (W_m) using the eel-like motion pattern. The work per meter was calculated according to

$$W_m = \frac{\int_0^T |\dot{\phi}\mathbf{u}|dt}{\sqrt{p_x^2 + p_y^2}}, \tag{43}$$

where T is the total simulated time and was set to 60s. Note that the eel-like motion was chosen as the gait to investigate the efficiency, since this is closer to the body undulation mode of a tunniform swimmer, which is well-known for its high speed and efficiency [9]. In particular, simulation results were obtained for eel-like motion with and without the caudal fin for different values of α_h, ω_h and δ_h. The work per meter as a function of the averaged forward speed are shown in Fig. 5, Fig. 6 and Fig. 7. The results presented in Fig. 5-7 for the investigated combinations of the gait parameters show that the snake robot with the caudal fin is more efficient with respect to work per meter than the robot without a fin. Note that the work per meter has a local minimum for the results with the caudal tail, which should be investigated further.

V. CONCLUSIONS

This article proposed a mathematical model for USRs which includes the extra propulsion forces acting on each link from different added effectors. The model is in closed form, and is thus well suited for control design and analysis. The USRs considered in this paper may be equipped with additional added effectors along their body, including caudal, dorsal and pectoral fins, tunnel thrusters and/or a stern propeller. In particular, the hydrodynamic model presented in [1] and [12] was extended to model the added mass effects more accurately, which afterwards was combined with the kinematic model to derive the closed form model of the USR. In addition, a quasi-static model for an oscillating and
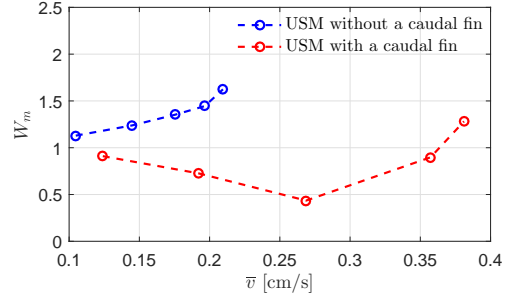

Fig. 5: The work per meter (W_m) as a function of the average forward velocity ($\bar{v}$) for different values of $\alpha_h = 15:5:35^o$, $\omega_h = 100^o/s$ and $\delta_h = 40^o$.
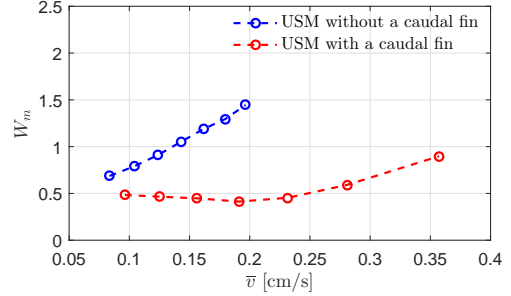

Fig. 6: The work per meter (W_m) as a function of the average forward velocity ($\bar{v}$) for different values of $\omega_h = 40:10:100^o/s$, $\alpha_h = 30^o$ and $\delta_h = 40^o$.

rotating foil was developed, which was then combined with the model of the USR to provide a model of an USR with one or more fins along its body. The resulting model kept the closed form property. Simulation results showed that there is a significant reduction in the work per meter for the USR with caudal (tail) fin compared to the results obtained for the USR without a caudal fin.

APPENDIX A

Matrices for the USR derived in Section II:

$$\mathbf{M_p} = \begin{bmatrix} m_{11} & m_{12} \\ m_{21} & m_{22} \end{bmatrix} = \begin{bmatrix} m_t + \mathbf{e}^T \mathbf{S}_\theta^2 \mu \mathbf{e} & -\mathbf{e}^T \mathbf{S}_\theta \mathbf{C}_\theta \mu \mathbf{e} \\ -\mathbf{e}^T \mathbf{S}_\theta \mathbf{C}_\theta \mu \mathbf{e} & m_t + \mathbf{e}^T \mathbf{C}_\theta^2 \mu \mathbf{e} \end{bmatrix}^{-1}$$

$$\mathbf{N_p} = \begin{bmatrix} \mathbf{e}^T \mathbf{S}_\theta \mathbf{C}_\theta \mu & \mathbf{e}^T \mathbf{S}_\theta^2 \mu \\ -\mathbf{e}^T \mathbf{C}_\theta^2 \mu & -\mathbf{e}^T \mathbf{S}_\theta \mathbf{C}_\theta \mu \end{bmatrix}$$

$$\mathbf{L_p} = \begin{bmatrix} \mathbf{e}^T \mathbf{S}_\theta^2 \mu & -\mathbf{e}^T \mathbf{S}_\theta \mathbf{C}_\theta \mu \\ -\mathbf{e}^T \mathbf{S}_\theta \mathbf{C}_\theta \mu & \mathbf{e}^T \mathbf{C}_\theta^2 \mu \end{bmatrix}$$
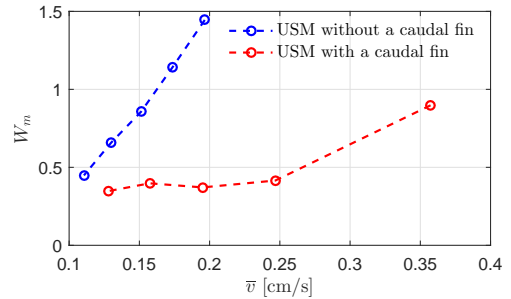

Fig. 7: The work per meter (W_m) as a function of the average forward velocity ($\bar{v}$) for different values of $\delta_h = 40:5:60^o$, $\alpha_h = 30^o$ and $\omega_h = 100^o/s$.

$$\mathbf{M}_\theta = \mathbf{J} + \mathbf{S}_\theta \mathbf{V}_1 \mathbf{S}_\theta + \mathbf{C}_\theta \mathbf{V}_1 \mathbf{C}_\theta - \mathbf{S}_\theta \bar{\mathbf{V}} \mathbf{A}_1 + \mathbf{C}_\theta \bar{\mathbf{V}} \mathbf{A}_4 + \mathbf{K}_5 \mathbf{K}_1 \bar{\mathbf{K}}^T \mathbf{S}_\theta$$
$$- \mathbf{K}_5 \mathbf{K}_2 \bar{\mathbf{K}}^T \mathbf{C}_\theta + \mathbf{K}_6 \mathbf{K}_3 \bar{\mathbf{K}}^T \mathbf{S}_\theta + \mathbf{K}_6 \mathbf{K}_4 \bar{\mathbf{K}}^T \mathbf{C}_\theta + \Lambda_1$$

$$\mathbf{W}_\theta = -\mathbf{S}_\theta \mathbf{V}_1 \mathbf{C}_\theta + \mathbf{C}_\theta \mathbf{V}_1 \mathbf{S}_\theta - \mathbf{S}_\theta \bar{\mathbf{V}} \mathbf{A}_2 + \mathbf{C}_\theta \bar{\mathbf{V}} \mathbf{A}_5 + \mathbf{K}_5 \mathbf{K}_1 \bar{\mathbf{K}}^T \mathbf{C}_\theta$$
$$+ \mathbf{K}_5 \mathbf{K}_2 \bar{\mathbf{K}}^T \mathbf{S}_\theta + \mathbf{K}_6 \mathbf{K}_3 \bar{\mathbf{K}}^T \mathbf{C}_\theta - \mathbf{K}_6 \mathbf{K}_4 \bar{\mathbf{K}}^T \mathbf{S}_\theta$$

$$\mathbf{V}_{\theta,\dot\theta} = -\mathbf{S}_\theta \bar{\mathbf{V}} \mathrm{diag}(\dot\theta)\mathbf{A}_3 + \mathbf{C}_\theta \bar{\mathbf{V}} \mathrm{diag}(\dot\theta)\mathbf{A}_6 - \mathbf{K}_5 \mathbf{K}_2 \mathrm{diag}(\dot\theta)\bar{\mathbf{K}}^T \mathbf{S}_\theta$$
$$- \mathbf{K}_5 \mathbf{K}_1 \mathrm{diag}(\dot\theta)\bar{\mathbf{K}}^T \mathbf{C}_\theta + \mathbf{K}_6 \mathbf{K}_4 \mathrm{diag}(\dot\theta)\bar{\mathbf{K}}^T \mathbf{S}_\theta$$
$$- \mathbf{K}_6 \mathbf{K}_3 \mathrm{diag}(\dot\theta)\bar{\mathbf{K}}^T \mathbf{C}_\theta + \Lambda_2 + \Lambda_3 \mathrm{diag}(|\dot\theta|)$$

$$\mathbf{N}_{\theta,\dot\theta} = \left(\mathbf{S}_\theta \bar{\mathbf{V}} \mathbf{S}_\theta \mathbf{C}_\theta \mu + \mathbf{C}_\theta \bar{\mathbf{V}} \mathbf{C}_\theta^2 \mu - \mathbf{K}_5 \mathbf{K}_2 + \mathbf{K}_6 \mathbf{K}_4 \right) \mathrm{diag}(\dot\theta)$$

$$\mathbf{P}_{\theta,\dot\theta} = \left(\mathbf{S}_\theta \bar{\mathbf{V}} \mathbf{S}_\theta^2 \mu + \mathbf{C}_\theta \bar{\mathbf{V}} \mathbf{S}_\theta \mathbf{C}_\theta \mu + \mathbf{K}_5 \mathbf{K}_1 + \mathbf{K}_6 \mathbf{K}_3 \right) \mathrm{diag}(\dot\theta)$$

$$\mathbf{K_x} = -\mathbf{S}_\theta \bar{\mathbf{V}} - \mathbf{K}_5 m_{11} \mathbf{e}^T - \mathbf{K}_6 m_{21} \mathbf{e}^T, \quad \mathbf{K_y} = \mathbf{C}_\theta \bar{\mathbf{V}} - \mathbf{K}_5 m_{12} \mathbf{e}^T - \mathbf{K}_6 m_{22} \mathbf{e}^T$$

$$\mathbf{A_1} = -\mathbf{S}_\theta^2 \mu \bar{\mathbf{K}}^T \mathbf{S}_\theta - \mathbf{S}_\theta \mathbf{C}_\theta \mu \bar{\mathbf{K}}^T \mathbf{C}_\theta, \quad \mathbf{A_2} = -\mathbf{S}_\theta^2 \mu \bar{\mathbf{K}}^T \mathbf{C}_\theta + \mathbf{S}_\theta \mathbf{C}_\theta \mu \bar{\mathbf{K}}^T \mathbf{S}_\theta$$
$$\mathbf{A_3} = -\mathbf{S}_\theta \mathbf{C}_\theta \mu \bar{\mathbf{K}}^T \mathbf{S}_\theta + \mathbf{S}_\theta^2 \mu \bar{\mathbf{K}}^T \mathbf{C}_\theta, \quad \mathbf{A_4} = \mathbf{S}_\theta \mathbf{C}_\theta \mu \bar{\mathbf{K}}^T \mathbf{S}_\theta + \mathbf{C}_\theta^2 \mu \bar{\mathbf{K}}^T \mathbf{C}_\theta$$
$$\mathbf{A_5} = \mathbf{S}_\theta \mathbf{C}_\theta \mu \bar{\mathbf{K}}^T \mathbf{C}_\theta - \mathbf{C}_\theta^2 \mu \bar{\mathbf{K}}^T \mathbf{S}_\theta, \quad \mathbf{A_6} = \mathbf{C}_\theta^2 \mu \bar{\mathbf{K}}^T \mathbf{S}_\theta - \mathbf{S}_\theta \mathbf{C}_\theta \mu \bar{\mathbf{K}}^T \mathbf{C}_\theta$$

$$\mathbf{K_1} = m_{11} \mathbf{e}^T \mathbf{S}_\theta^2 \mu - m_{12} \mathbf{e}^T \mathbf{S}_\theta \mathbf{C}_\theta \mu, \quad \mathbf{K_2} = -m_{11} \mathbf{e}^T \mathbf{S}_\theta \mathbf{C}_\theta \mu + m_{12} \mathbf{e}^T \mathbf{C}_\theta^2 \mu$$
$$\mathbf{K_3} = m_{21} \mathbf{e}^T \mathbf{S}_\theta^2 \mu - m_{22} \mathbf{e}^T \mathbf{S}_\theta \mathbf{C}_\theta \mu, \quad \mathbf{K_4} = m_{21} \mathbf{e}^T \mathbf{S}_\theta \mathbf{C}_\theta \mu - m_{22} \mathbf{e}^T \mathbf{C}_\theta^2 \mu$$
$$\mathbf{K_5} = -\mathbf{S}_\theta \mathbf{V}_2 - \mathbf{S}_\theta \bar{\mathbf{V}} \mathbf{S}_\theta^2 \mu \mathbf{e} - \mathbf{C}_\theta \bar{\mathbf{V}} \mathbf{S}_\theta \mathbf{C}_\theta \mu \mathbf{e}$$
$$\mathbf{K_6} = \mathbf{C}_\theta \mathbf{V}_2 + \mathbf{S}_\theta \bar{\mathbf{V}} \mathbf{S}_\theta \mathbf{C}_\theta \mu \mathbf{e} + \mathbf{C}_\theta \bar{\mathbf{V}} \mathbf{C}_\theta^2 \mu \mathbf{e}$$

Matrices for the combined model of USR and foil model:

$$\mathbf{K_p} = \left[\begin{array}{c} \mathbf{e}^T \mathbf{S}_{\psi+\beta} \pi \rho \mathbf{S} \mathbf{B}^3 \alpha \\ \mathbf{e}^T \mathbf{C}_{\psi+\beta} \pi \rho \mathbf{S} \mathbf{B}^3 \alpha \end{array} \right]$$

$$\mathbf{S_p} = \left[\begin{array}{cc} s_{11} & s_{12} \\ s_{21} & s_{22} \end{array} \right] = \left[\begin{array}{cc} \mathbf{e}^T \mathbf{S}_{\psi+\beta} \pi \rho \mathbf{S} \mathbf{B}^2 \mathbf{S}_\psi & \mathbf{e}^T \mathbf{S}_{\psi+\beta} \pi \rho \mathbf{S} \mathbf{B}^2 \mathbf{C}_\psi \\ \mathbf{e}^T \mathbf{C}_{\psi+\beta} \pi \rho \mathbf{S} \mathbf{B}^2 \mathbf{S}_\psi & \mathbf{e}^T \mathbf{C}_{\psi+\beta} \pi \rho \mathbf{S} \mathbf{B}^2 \mathbf{C}_\psi \end{array} \right]$$

$$\mathbf{M_p^t} = \left[\begin{array}{cc} m_{11} & m_{12} \\ m_{21} & m_{22} \end{array} \right] = \left[\begin{array}{cc} m_t + \mathbf{e}^T \mathbf{S}_\theta^2 \mu \mathbf{e} + s_{11} \mathbf{e} & -\mathbf{e}^T \mathbf{S}_\theta \mathbf{C}_\theta \mu \mathbf{e} + s_{12} \mathbf{e} \\ -\mathbf{e}^T \mathbf{S}_\theta \mathbf{C}_\theta \mu \mathbf{e} + s_{21} \mathbf{e} & m_t + \mathbf{e}^T \mathbf{C}_\theta^2 \mu \mathbf{e} + s_{22} \mathbf{e} \end{array} \right]^{-1}$$

$$\mathbf{M}_\theta^t = \mathbf{M}_\theta - \mathbf{B}_1^t + (\mathbf{K}_5 + \mathbf{B}_3^t)(\mathbf{N}_5 + \mathbf{N}_7) + (\mathbf{K}_6 + \mathbf{B}_4^t)(\mathbf{N}_6 + \mathbf{N}_8)$$
$$+ \mathbf{B}_3^t (\mathbf{K}_1 \bar{\mathbf{K}}^T \mathbf{S}_\theta - \mathbf{K}_2 \bar{\mathbf{K}}^T \mathbf{C}_\theta) + \mathbf{B}_4^t (\mathbf{K}_3 \bar{\mathbf{K}}^T \mathbf{S}_\theta + \mathbf{K}_4 \bar{\mathbf{K}}^T \mathbf{C}_\theta)$$
$$\mathbf{W}_\theta^t = \mathbf{W}_\theta - \mathbf{B}_2^t + (\mathbf{K}_5 + \mathbf{B}_3^t)\mathbf{N}_9 + (\mathbf{K}_6 + \mathbf{B}_4^t)\mathbf{N}_{10}$$
$$+ \mathbf{B}_3^t (\mathbf{K}_1 \bar{\mathbf{K}}^T \mathbf{C}_\theta + \mathbf{K}_2 \bar{\mathbf{K}}^T \mathbf{S}_\theta) + \mathbf{B}_4^t (\mathbf{K}_3 \bar{\mathbf{K}}^T \mathbf{C}_\theta - \mathbf{K}_4 \bar{\mathbf{K}}^T \mathbf{S}_\theta)$$
$$\mathbf{V}_{\theta,\dot\theta}^t = \mathbf{V}_{\theta,\dot\theta} - \mathbf{B}_3^t (\mathbf{K}_2 \mathrm{diag}(\dot\theta)\bar{\mathbf{K}}^T \mathbf{S}_\theta + \mathbf{K}_1 \mathrm{diag}(\dot\theta)\bar{\mathbf{K}}^T \mathbf{C}_\theta)$$
$$+ \mathbf{B}_4^t (\mathbf{K}_4 \mathrm{diag}(\dot\theta)\bar{\mathbf{K}}^T \mathbf{S}_\theta - \mathbf{K}_3 \mathrm{diag}(\dot\theta)\bar{\mathbf{K}}^T \mathbf{C}_\theta)$$
$$\mathbf{N}_{\theta,\dot\theta}^t = \mathbf{N}_{\theta,\dot\theta} + (-\mathbf{B}_3^t \mathbf{K}_2 + \mathbf{B}_4^t \mathbf{K}_4)\mathrm{diag}(\dot\theta)$$
$$\mathbf{P}_{\theta,\dot\theta}^t = \mathbf{P}_{\theta,\dot\theta} + (\mathbf{B}_3^t \mathbf{K}_1 + \mathbf{B}_4^t \mathbf{K}_3)\mathrm{diag}(\dot\theta)$$

$$\mathbf{K_x^t} = \mathbf{K_x} - \mathbf{B}_3^t m_{11} \mathbf{e}^T - \mathbf{B}_4^t m_{12} \mathbf{e}^T, \quad \mathbf{K_y^t} = \mathbf{K_y} - \mathbf{B}_3^t m_{21} \mathbf{e}^T - \mathbf{B}_4^t m_{22} \mathbf{e}^T$$

$$\mathbf{B_1^t} = \mathbf{S}_\theta \bar{\mathbf{V}} \mathbf{S}_{\beta_\psi} \mathbf{N}_1 - \mathbf{C}_\theta \bar{\mathbf{V}} \mathbf{C}_{\beta_\psi} \mathbf{N}_1 + \mathbf{P}_1$$
$$\mathbf{B_2^t} = \mathbf{S}_\theta \bar{\mathbf{V}} \mathbf{S}_{\beta_\psi} \mathbf{N}_2 - \mathbf{C}_\theta \bar{\mathbf{V}} \mathbf{C}_{\beta_\psi} \mathbf{N}_2 + \mathbf{P}_2$$
$$\mathbf{B_3^t} = -\mathbf{S}_\theta \bar{\mathbf{V}} \mathbf{S}_{\beta_\psi} \mathbf{N}_3 + \mathbf{C}_\theta \bar{\mathbf{V}} \mathbf{C}_{\beta_\psi} \mathbf{N}_3 + \mathbf{S} \pi \rho \mathbf{B}^3 \alpha \mathbf{S}_\psi \mathbf{e}$$
$$\mathbf{B_4^t} = -\mathbf{S}_\theta \bar{\mathbf{V}} \mathbf{S}_{\beta_\psi} \mathbf{N}_4 + \mathbf{C}_\theta \bar{\mathbf{V}} \mathbf{C}_{\beta_\psi} \mathbf{N}_4 + \mathbf{S} \pi \rho \mathbf{B}^3 \alpha \mathbf{C}_\psi \mathbf{e}$$

$$\mathbf{N_1} = \pi \rho \mathbf{S}(\mathbf{B}^2 \mathbf{S}_\psi \bar{\mathbf{K}}^T \mathbf{S}_\theta - \mathbf{B}^2 \mathbf{C}_\psi \bar{\mathbf{K}}^T \mathbf{C}_\theta - \mathbf{B}^3 \alpha), \quad \mathbf{N_3} = -\pi \rho \mathbf{S} \mathbf{B}^2 \mathbf{S}_\psi \mathbf{e}$$
$$\mathbf{N_2} = \pi \rho \mathbf{S} \mathbf{B}^2 (\mathbf{S}_\psi \bar{\mathbf{K}}^T \mathbf{C}_\theta + \mathbf{C}_\psi \bar{\mathbf{K}}^T \mathbf{S}_\theta), \quad \mathbf{N_4} = -\pi \rho \mathbf{S} \mathbf{B}^2 \mathbf{C}_\psi \mathbf{e}$$
$$\mathbf{N_5} = (m_{11} \mathbf{e}^T \mathbf{S}_{\beta_\psi} + m_{12} \mathbf{e}^T \mathbf{C}_{\beta_\psi}) \pi \rho \mathbf{S} \mathbf{B}^3 \alpha$$
$$\mathbf{N_6} = (m_{21} \mathbf{e}^T \mathbf{S}_{\beta_\psi} + m_{22} \mathbf{e}^T \mathbf{C}_{\beta_\psi}) \pi \rho \mathbf{S} \mathbf{B}^3 \alpha$$
$$\mathbf{N_7} = m_{11}(s_{11} \bar{\mathbf{K}}^T \mathbf{S}_\theta - s_{12} \bar{\mathbf{K}}^T \mathbf{C}_\theta) + m_{12}(s_{21} \bar{\mathbf{K}}^T \mathbf{S}_\theta - s_{22} \bar{\mathbf{K}}^T \mathbf{C}_\theta)$$
$$\mathbf{N_8} = m_{21}(s_{11} \bar{\mathbf{K}}^T \mathbf{S}_\theta - s_{12} \bar{\mathbf{K}}^T \mathbf{C}_\theta) + m_{22}(s_{21} \bar{\mathbf{K}}^T \mathbf{S}_\theta - s_{22} \bar{\mathbf{K}}^T \mathbf{C}_\theta)$$
$$\mathbf{N_9} = m_{11}(s_{11} \bar{\mathbf{K}}^T \mathbf{C}_\theta + s_{12} \bar{\mathbf{K}}^T \mathbf{S}_\theta) + m_{12}(s_{21} \bar{\mathbf{K}}^T \mathbf{C}_\theta + s_{22} \bar{\mathbf{K}}^T \mathbf{S}_\theta)$$
$$\mathbf{N_{10}} = m_{21}(s_{11} \bar{\mathbf{K}}^T \mathbf{C}_\theta + s_{12} \bar{\mathbf{K}}^T \mathbf{S}_\theta) + m_{22}(s_{21} \bar{\mathbf{K}}^T \mathbf{C}_\theta + s_{22} \bar{\mathbf{K}}^T \mathbf{S}_\theta)$$

$$\mathbf{P_1} = -\mathbf{S} \pi \rho \mathbf{B}^4 \left(\frac{1}{8} \mathbf{I}_n + \alpha^2 \right) + \mathbf{S} \pi \rho \mathbf{B}^3 \alpha (\mathbf{S}_\psi \bar{\mathbf{K}}^T \mathbf{S}_\theta - \mathbf{C}_\psi \bar{\mathbf{K}}^T \mathbf{C}_\theta)$$
$$\mathbf{P_2} = \mathbf{S} \pi \rho \mathbf{B}^3 \alpha (\mathbf{S}_\psi \bar{\mathbf{K}}^T \mathbf{C}_\theta + \mathbf{C}_\psi \bar{\mathbf{K}}^T \mathbf{S}_\theta)$$

REFERENCES

[1] J. Sverdrup-Thygeson, E. Kelasidi, K. Y. Pettersen, and J. T. Gravdahl, "Modeling of underwater swimming manipulators," in *Proc.10th IFAC Conference on Control Applications in Marine Systems (CAMS)*, Trondheim, Norway, Sept. 13-16 2016, pp. 81–88.

[2] ——, "A control framework for biologically inspired underwater swimming manipulators equipped with thrusters," in *Proc.10th IFAC Conference on Control Applications in Marine Systems (CAMS)*, Trondheim, Norway, Sept. 13-16 2016, pp. 89–96.

[3] ——, "The underwater swimming manipulator - a bio-inspired auv," in *Proc. IEEE/OES Autonomous Underwater Vehicles (AUV)*, Tokyo, Japan, Nov. 6-9 2016, pp. 387–395.

[4] P. Ridao, M. Carreras, D. Ribas, P. Sanz, and G. Oliver, "Intervention AUVs: The Next Challenge," in *Proc. 19th IFAC World Congress (IFAC-WC)*, Cape Town, South Africa, Aug. 24-29 2014, pp. 12 146–12 159.

[5] E. Kelasidi, P. Liljebäck, K. Y. Pettersen, and J. T. Gravdahl, "Innovation in underwater robots: Biologically inspired swimming snake robots," *IEEE Robotics and Automation Magazine*, vol. 23, no. 1, pp. 44–62, 2016.

[6] E. Kelasidi, K. Y. Pettersen, P. Liljebäck, and J. T. Gravdahl, "Locomotion efficiency of underwater snake robots with thrusters," in *Proc. IEEE Inter. Symposium on Safety, Security, and Rescue Robotics (SSRR)*, Lausanne, Switzerland, Oct. 23 - 27 2016, pp. 174–181.

[7] S. Lighthill, *Mathematical Biofluiddynamics*. Society for Industrial and Applied Mathematics, 1975.

[8] M. J. Lighthill, "Aquatic animal propulsion of high hydro-mechanical efficiency," *Journal of Fluid Mechanics*, vol. 44, no. 2, pp. 265–301, 1970.

[9] S. Strømsøyen, "Propulsion methods for under water snake robots - investigation and simulation using foil for propulsion of a snake robot," in *MSc thesis, NTNU*, 2015.

[10] M. Triantafyllou and G. Triantafyllou, "An efficient swimming machine," *Scientific American*, vol. 272, no. 3, pp. 40–48, 1995.

[11] M. Triantafyllou, G. Triantafyllou, and D. Yue, "Hydrodynamics of fishlike swimming," *Annual review of fluid mechanics*, vol. 32, no. 1, pp. 33–53, 2000.

[12] E. Kelasidi, K. Y. Pettersen, J. T. Gravdahl, and P. Liljebäck, "Modeling of underwater snake robots," in *Proc. IEEE International Conference on Robotics and Automation (ICRA)*, Hong Kong, China, May 31-June 7 2014, pp. 4540–4547.

[13] E. Kelasidi, K. Y. Pettersen, P. Liljebäck, and J. T. Gravdahl, "Integral line-of-sight for path-following of underwater snake robots," in *Proc. IEEE Multi-Conference on Systems and Control*, Antibes, France, Oct. 8-10 2014, pp. 1078 – 1085.

[14] P. Liljebäck, K. Y. Pettersen, Ø. Stavdahl, and J. T. Gravdahl, *Snake Robots: Modelling, Mechatronics, and Control*. Springer-Verlag, Advances in Industrial Control, 2013.

[15] P. Liljebäck, Ø. Stavdahl, K. Pettersen, and J. Gravdahl, "Mamba - a waterproof snake robot with tactile sensing," in *Proc. International Conference on Intelligent Robots and Systems (IROS)*, Chicago, IL, Sept. 14-18 2014, pp. 294–301.

[16] M. Sfakiotakis, D. M. Lane, and J. B. C. Davies, "Review of fish swimming modes for aquatic locomotion," *IEEE Journal of Oceanic Engineering*, vol. 24, no. 2, pp. 237–252, 1999.

[17] P. Webb, *Hydrodynamics and Energetics of Fish Propulsion*, B. F. R. B. of Canada), Ed. Department of the Environment Fisheries and Marine Service, 1975.

[18] M. Kruusmaa, P. Fiorini, W. Megill, M. De Vittorio, O. Akanyeti, F. Visentin, L. Chambers, H. El Daou, M.-C. Fiazza, J. Jezov, M. Listak, L. Rossi, T. Salumae, G. Toming, R. Venturelli, D. Jung, J. Brown, F. Rizzi, A. Qualtieri, J. Maud, and A. Liszewski, "Filose for svenning: A flow sensing bioinspired robot," *IEEE Robotics Automation Magazine*, vol. 21, no. 3, pp. 51–62, 2014.

[19] J. G. Leishman, *Principles of Helicopter Aerodynamics*, C. U. Press, Ed. Part of Cambridge Aerospace Series, 2006.

[20] S. Steen, *Foil and propeller theory*. Department of marine technology, NTNU, 2014.

[21] O. Faltinsen, *Hydrodynamics of High-Speed Marine Vehicles*. Cambridge University Press, 2005.

[22] J. Newman, *Marine Hydrodynamics*. MIT Press, 1977.

[23] E. Kelasidi, P. Liljebäck, K. Y. Pettersen, and J. T. Gravdahl, "Integral line-of-sight guidance for path following control of underwater snake robots: Theory and experiments," *IEEE Transactions on Robotics*, vol. PP, no. 99, pp. 1–19, 2017, DOI:10.1109/TRO.2017.2651119.